Investigation of ionic local structure in molten salt fast reactor LiF-ThF4-UF4 fuel by EXAFS experiments and molecular dynamics simulations

Catherine Bessada, Didier Zanghi, Mathieu Salanne, Ana Gil-Martin, Mathieu Gibilaro, Pierre Chamelot, Laurent Massot, Atsushi Nezu, Haruaki Matsuura

Investigation of ionic local structure in molten salt fast reactor LiF-ThF_4-UF_4 fuel by EXAFS experiments and molecular dynamics simulations

Catherine Bessada[1*], Didier Zanghi[1], Mathieu Salanne[2], Ana Gil-Martin[1,3], Mathieu Gibilaro[4], Pierre Chamelot[4], Laurent Massot[4], Atsushi Nezu[5], Haruaki Matsuura[6]

[1]*CNRS, CEMHTI UPR3079, Univ. Orléans, F-45071 Orléans, France*

[2]*Sorbonne Univ., UPMC Univ. Paris 06, CNRS, PHENIX, F-75005 Paris- France*

[3] *Enusa Industrias Avanzadas, S.A. 28040-Madrid*

[4]*LGC Univ Toulouse Laboratoire de Génie Chimique UMR 5503 Université de Toulouse III Paul Sabatier 31062 Toulouse cedex 4,*

[5]*RLNR, Tokyo Institute of Technology, Tokyo 152-8550, Japan*

[6]*Tokyo City University, Department of Nuclear Safety Engineering & Cooperative Major in Nuclear Energy, Tokyo 158-8557, Japan*

Keywords: EXAFS, Molecular dynamics, high temperature, molten salt reactors, speciation, actinides

Abstract

This article focuses on the speciation of molten fluoride mixtures based on ThF_4 and UF_4 actinides used in molten salt reactors. The local structure of molten AF-MF_4 systems (A=Li^+, Na^+, K^+; M= Th^{4+}, U^{4+}) was studied in situ by combining measurements by high temperature X-ray absorption spectroscopy and molecular dynamics simulations. In the molten state, 20°C higher than the melting temperature, these mixtures are composed of free fluorine and anionic species $[MF_7]^{3-}$, $[MF_8]^{4-}$ and $[MF_9]^{5-}$ whose distribution varies with the amount of MF_4 (M= Th^{4+}, U^{4+}). Regardless of the cation, these complexes consist of an average of 8 F^- neighbors for MF_4 content is less than 35 mol. %. This value decreases to 7 as the size of the alkaline ion A (A=Li^+, Na^+, K^+) increases. The $[MF_x]^{4-x}$ species are linked together by bridging fluorine ions to form long chains $[M_xF_Y]^{4x-y}$. The addition of a few percent UF_4 to the eutectic LiF-ThF_4 composition (77.5 mol% - 22.5 mol. %) at 700°C leads to a slight increase in the population of free fluorine ions due to the breakdown of the Th-F links to form complexes $[UF_x]^{4-x}$ isolated or connected to the $(Th_xF_y)^{4x-y}$ chains. This change in the structure of the liquid results in a slight decrease in viscosity when a few mol. % of UF_4 is added.

1. Introduction

At long time scales, the majority of the radioactivity in nuclear waste comes from actinide elements. Reducing the amount of actinide waste produced and developing long-term storage methods are critical issues affecting the long-term viability of the nuclear power industry. It is thus necessary to investigate new fuel cycles that reduce the amount of actinide and one promising advanced fuel cycle option is the molten salt fast reactor (MSFR) [1].

This concept consists in a liquid molten fluoride salt used as coolant and fuel, circulating in a loop around the reactor, and in situ reprocessed by electrochemistry to extract the fission products. Various mixtures of UF_4 and ZrF_4 fuels were first considered in the reactor designed in the laboratory of Oak Ridge [2]. Nowadays, the researches focus on reactors operating with fast neutron spectrum, which do not require a moderator material. The fuel is a mixture of LiF-ThF_4 at eutectic composition (77.5 mol. % - 22.5 mol. %) with addition of UF_4 (3 mol. %) to start the nuclear reactions [3]. Salt composition has significant effects on neutronics, thermal-hydraulics and corrosion properties of the molten salt reactors [4]. Furthermore, the transport properties, in particular the viscosity, are directly correlated to the liquid structure. Due to production of fission products (FP) and minor actinides during the operating cycle, it is important to characterize the anionic complexes involved in the molten fluorides mixtures on a wide range of compositions and temperatures. For all these reasons, a precise description of the liquid structure is needed to determine their speciation in the media.

The LiF-ThF_4 binary system is a key system for various designs of the MSFRs. To determine the operation parameters and the safety limit of the reactor, physico-chemical properties of this molten salt have been recently reassessed by Capelli *et al.* [5], such as the vapor pressure of LiF and ThF_4 in liquid solution. The physical properties, such as volume expansion, density [6], ionic mobility [7], electrical conductivity [8] or viscosity [9], were obtained by experimental methods or calculations. Likewise, the electrochemistry of thorium halides was studied to develop the reprocessing processes [10-13].

However, the structural description of molten fluorides at high temperature is less common, due to inherent experimental difficulties. These constraints require developing specific cells and appropriate heating systems to perform in *situ* measurements. High Temperature Raman spectroscopy was used to describe the local structure of molten thorium fluorides [14]. For example, Toth *et al.* showed the presence of $[ThF_8]^{4-}$ and $[ThF_7]^{3-}$ species in LiF-NaF-ThF_4 mixture [15]. More recently, Bessada *et al.* [16] followed by Smith *et al.* [17], developed a new set-up and a sample containment cell for measuring local structure of

radioactive molten fluorides AF-ThF_4 (A^+= K^+, Li^+) by extended X-ray absorption fine structure (EXAFS) at the L_3 threshold of the thorium. This spectroscopic technique, sensitive to the local environment around a given element, is well adapted to obtain qualitative and quantitative information on the first solvation shell of heavy cations such as thorium. These authors demonstrated the formation of Th-based anionic complexes $[ThF_7]^{3-}$, $[ThF_8]^{4-}$, $[ThF_9]^{5-}$ isolated or connected by bridging F^- in KF-ThF_4 (75-25 mol. %) system at 900°C and LiF-ThF_4 (50-50 mol. %) mixture at 920°C, combining high temperature EXAFS data and molecular dynamics (MD) simulations. The same approach was adopted to investigate the local structure of the molten ThF_4-LiF and ThF_4-LiF- BeF_2 mixtures. Experiments performed by Sun *et al.* [18] and calculations realized by Dai and co-workers [19] confirm the tendencies observed and show that the addition of beryllium ions in these molten systems increases the structural disorder around thorium ions.

In addition to these experimental measurements, Dewan *et al.* [20] studied, by classical molecular dynamics simulations with a polarizable ion model (PIM) [21-22], the structural organization and transport properties on LiF-ThF_4 molten salt at the eutectic composition. They calculated the self-diffusion coefficients and the viscosity as well as the changes of the coordination number of Th^{4+} over a temperature range from 580°C to 1000°C. The thermophysical properties of LiF-ThF_4 mixtures were calculated for a wide range of compositions and temperatures by Gheribi *et al.* [23]. By using the same potential, Liu and co-workers [24] completed this study by performing calculations on a whole range of compositions (5 mol. % - 65 mol. %) and temperatures (830°C – 1130°C). They examined the evolution of $[ThF_n]^{4-n}$ complexes (n = 7, 8, 9) and found that the average coordination number with the composition of the melt is around 8 ± 1. With a lifetime of a few picoseconds, the coordination shell of Th^{4+} ions is more transient than that of Zr^{4+} ions in presence of LiF. This study was recently completed by calculation in the AF-ThF_4 molten system (A^+= Li^+, Na^+ and K^+) of the effect of the size of alkaline A^+ on the electronic structure of $[ThA_8F_8]^{4+}$ complexes and on macroscopic thermo-physical macroscopic properties such as thermal expansions and mass enthalpies [25].

In this article, the structure of molten AF-ThF_4 (A^+=Li^+, Na^+, K^+) and LiF-UF_4 binary systems were investigated, which are fuel salt compositions used on the front end of the nuclear fuel cycle in MSRs. The objective is to investigate the structural description around the tetravalent cations by changing the nature of the alkali and to experimentally evidence the existence of bridging fluorine ions between the species, forming a “network” when a small quantity of UF_4 is added to LiF-ThF_4.

2. Experiments and Calculations

2.1 Samples preparation

Samples were prepared and packed in a glovebox dedicated to radioactive elements, under a dried argon atmosphere to prevent air oxidation. Different compositions of fluorides mixtures UF_4-LiF, ThF_4-LiF and $[ThF_4\text{-LiF}]_{eutectic}$ + UF_4 were prepared for EXAFS experiments.

For AF-ThF_4 (A=Li^+, Na^+, K^+) fluoride salts, pure ThF_4 was synthesized at Tohoku University by Professor Sato. It was produced by a hydro-fluorination of ThO_2 under Ar and F_2 (10% diluted with Helium gaz) atmosphere in a nickel boat at 600°C for three hours. Mixtures of ThF_4 and alkali metal fluorides (LiF, NaF and KF) were made by reaction at 500°C for 30 hours under argon atmosphere in a nickel nacelle. For each steps of preparation, crystallographic phases were controlled to ensure a good purity.

Preparation of LiF-UF_4 and $[LiF\text{-}ThF_4]_{eut}$ + UF_4 samples was carried out at LGC laboratory in Toulouse. For LiF-ThF_4 or LiF-UF_4 eutectic composition, ThF_4 was purchased from American Elements (99.9 % pure), UF_4 from Areva (99.9 % pure) and LiF from Carlo Erba (99.99 % pure) and they were manually grinded.

Then, they were mixed with boron nitride (BN) powder and pressed under 1ton cm^{-2} into pellets of 7 mm diameter and 500 µm thickness. BN powder plays an essential role here: once compacted, it produces an inert microporous matrix in which the salt in the molten state is confined in the form of micro-droplets, homogeneously dispersed in the matrix above its melting point.

Pellets were inserted in two pyrolitic boron nitride (PBN) plates [26] able to resist up to 1800°C under inert atmosphere. The PBN cell is composed of a two-face round plates closed with 6 screws to avoid molten fluoride leakage and constitutes a second containment barrier. This cell is introduced in a 25mm height cylindrical cell, used as a third confinement barrier to prevent radiological contamination of the furnace [27]. The geometry of the cylinder is well adapted for EXAFS measurements in a transmission mode, allowing to probe relatively concentrated samples with a good signal-to-noise ratio. Moreover, it does not require to correct the signals of reabsorption phenomena that may occur when detecting the EXAFS signal by measuring fluorescence X-rays.

2.2 EXAFS measurements

EXAFS experiments were carried out on the BL27B beamline of the Photon Factory (PF) KeK [28] in Tsukuba (Japan). The scans in energy were performed in transmission geometry with a double crystals Si (111) monochromator. Two ionization chambers were used and filled with N_2 for detection of incident photons, and with N_2-Ar (50%) for transmitted photons. The beam was sized with slits to obtain a rectangular spot size of 3 mm vertically and 5 mm horizontally. Fixed time scanning (1 s/point) was performed in the energy range 16.2-17.4 keV at the L_{III} absorption edges of Th (16.3 keV) and 17.0 to 18.3 keV at the L_{III} absorption edges of U (17.166 keV). To minimize the collection time, the energy range was divided into four areas by using an energy step of 4 eV for the first and the fourth zone, 1 eV for the absorption edge and 2 eV for the third zone.

The furnace developed by Rigaku Corp. in Japan is composed of two heating elements made of alumina plates surrounded by a wire Pt-Rh20%. The Kapton windows were replaced by windows of Beryllium, transparent to X-rays and more resistant to the constraints. The heating chamber is cooled by water circulation and allows to work under a low pressure of helium during experiment to confine the sample. Thanks to all these modifications, this chamber can figure an additional barrier in the extreme case that radioactive material would pass through the first three barriers during the experiment.

A 10 K/min heating ramp was applied to heat the samples from room temperature to 975K with dwell time of one hour at 775 K and 875 K to collect EXAFS data. The EXAFS oscillations were extracted by using Athena software [29].

2.3 Molecular dynamic calculations

The molecular dynamics (MD) simulations were performed on the actinides fluorides systems in the framework of a polarizable ion model (PIM) [21-22]. The classical interaction potential derived from this model is well adapted to describe the ionic interactions in the molten fluorides [20, 30, 31]. The total potential is built from the addition of ionic pairs. The contribution for each pairs is a sum of three terms (charge-charge, dispersion, and overlap repulsion) similar to a Born-Mayer pair potential, plus an additional term taking into account the ionic polarization. Each contribution is described by a set of parameters determined from

first-principles calculations [32] using an iterative fitting procedure [33, 34]. The parameter values for the LiF-ThF_4, LiF-UF_4 and $[LiF\text{-}ThF_4]_{eutectic}$ + UF_4 systems are given in references [20, 35]. They have been developed for the binary systems LiF-ThF_4 and LiF-UF_4. In the case of Th^{4+}-Th^{4+} and U^{4+}-U^{4+} pairs, the values of these parameters are effectively identical because these 2 ions are comparable in terms of oxidation state, radius, mass and atomic number and electronegativity. It is for this reason that we considered that it was the same for the Th^{4+}-U^{4+} pair during the study of the ternary ThF_4-LiF-UF_4 system. The parameters were validated using transport properties (self-diffusion coefficients, electrical conductivity, viscosity and heat capacity) in a large range of temperatures and compositions, and compared to experimental data.

MD simulations were carried out with a time step of 0.5 fs in two stages. A first series of calculations were performed in the NPT ensemble during 0.2 ns to determine the equilibrium density of the (N) particles included in the cubic simulation cell maintained in a pressure (P) of 1 atmosphere and a target temperature (T), thanks to a barostat and a thermostat where the relaxation times were set to 0.01 ns. Then, a second series of computations were performed in the NVT ensemble where the cell volume (V) is fixed by removing the barostat. In this second stage, the atomic configurations are stored every 0.1 ps during the simulation time during 5 ns. This duration is sufficient to evaluate the transport properties such as the viscosity and the self-diffusion coefficients (without external electric fields). All the simulated systems are described (number of ions, volume of the cell) in Tables 1-3.

2.4 FEFF computations

In previous studies [30], atomic configurations obtained from the molecular dynamics trajectories for a given temperature were used as input data in the EXAFS simulation code FEFF [36] to calculate EXAFS oscillations ($\chi(k)$) for a given absorption edge (L3 edges of Th or U).

The Cartesian coordinates of ions in the simulation cell are used to define a cluster centered on a specific absorber atom (Th^{4+} or U^{4+} ions) in order to calculate the multiple photo-electron backscattering contributions to the EXAFS signal arising out of its neighbor atoms. However, as in the liquid the main contribution results in the single backscattering paths from the first neighbors, the FEFF calculations were performed with a number of

backscattering paths limited to 4 and a half-path distance set to 9 Å to include the full second coordination shell.

Accumulation of FEFF computations on the whole clusters and on atomic configurations leads to an average EXAFS curve which can be compared directly to the EXAFS oscillations extracted from the experimental data. Typically, FEFF calculations were carried out on an average of 40,000 different atomic configurations, which is necessary to have a good description of the local structure around a given ion. Moreover, the statistical analysis of the EXAFS spectrum for each cluster enables to determine quantitatively the contribution from the different coordination number of the absorber's environment to the average EXAFS signal. Thanks to this decomposition, distribution of the coordination and the average distance of the formed complexes can be determined.

3. Results

3.1 Molten MF-ThF_4 systems (M=Li, Na, K)

In this part, EXAFS experiments carried out at the L_3 edge of Th (16.3 keV) on LiF-ThF_4 compounds are presented. Among the different mixtures in this binary system, three compositions with increasing content of thorium tetrafluoride (18, 25 and 35 mole % of ThF4) around the eutectic compositions were selected. Figure 1 reports the Fourier transform of the EXAFS signals recorded at room temperature and 975 K for the 25 mol.% ThF – 75 mol. % LiF compound. The first peak observed on both spectra points out the existence of a local order near the thorium (IV) ions. The magnitude of this peak is proportional to their nearest neighbors. In the monoclinic ThF_4 solid phase, Th^{4+} ions are 8-fold coordinated with F^- anions at an average distance of 2.34 Å [37]. The shift of that peak toward greater distances as temperature increases reflects a dilatation of Th-F bonding at high temperature due to thermal and topological disorder effects. As this disorder results in an exponential damping of the EXAFS signal, it leads to a decrease in the amplitude of the first peak and the disappearance of the second peak at 4.4 Å which indicates the loss of a large range order in the local structure around thorium atoms, typical of a liquid phase.

For such disordered systems, quantitative analysis of EXAFS data required to take into account the distribution of atomic environments around a selected atomic species. To investigate Th^{4+} short-range order, this liquid was modeled and generated by molecular

dynamics simulations to calculate the corresponding k^2 weighted EXAFS data (k^2 $\chi(k)$) with the FEFF program by considering only 40000 atomic configurations. Previous work [30,38] showed that this number was sufficient to fit the experimental data.

The comparison between calculated oscillations and experimental curves extracted from the measured absorption coefficient μ(E) above the thorium L3 absorption edge is presented on Figure 2. For the three studied compositions (82%LiF-18%ThF_4, 75%LiF-25%ThF_4, 65%LiF-35%ThF_4) in the liquid phase at high temperature (700°C), the EXAFS signal is formed by a damped sinusoidal oscillation with a small peak superimposed to the main oscillation at 10.3 $Å^{-1}$. This later can be attributed to a double-electron excitation phenomenon, specific in the L3-edge x-ray absorption spectra of actinides [39]. Except this anomaly which is not taken into account in the FEFF calculations, amplitude and frequency of the EXAFS signals are well reproduced on a wide range of wave numbers k. Even if the ab initio parametrized interaction potential used in this study was already successfully applied to reproduce thermodynamic and transport data [20], this result confirms that it is also able to describe the structure of such ionic liquid systems.

The total signal generated by calculation is the sum of three contributions. Every single contribution corresponds to the average EXAFS signal of three $[ThF_n]^{4-n}$ complexes (n=7, 8, 9) whose amplitude reflects the distribution of the coordination number n and the signal frequency, the average distance Th-F for each complex. On Figure 3 is presented the EXAFS signal decomposition obtained for LiF-ThF_4 (75 mol. % - 25 mol. %) at 700°C. The majority of the EXAFS signal is due to the presence of 59 % of $[ThF_8]^{4-}$ species with an average (Th-F) distance of 2.35 Å. For $[ThF_7]^{3-}$ and $[ThF_9]^{5-}$ complexes, the average distances (Th-F) are 2.29 Å and 2.41 Å respectively, accounting for 22 % and 17 % of the total signal (Table 4). These results are in agreement with MD computations performed on LiF-ThF_4 structure at 1200 K [20, 23, 24] and high temperature Raman measurements [14, 15]. These works also highlighted the existence of these three complexes and the fact that anionic species $[ThF_8]^{4-}$ were in the majority over a composition range from 5 mol. % to 70 mol. % of ThF_4.

Then, the effect of composition by systematically working 20°C above the melting temperature was investigated. The statistical analysis of ionic trajectories produced by MD simulations allowed to follow the evolution of these complexes as function of the temperature and the composition. The coordination number (CN) is calculated from the first solvation shell of Th^{4+}, defined by a cutoff distance corresponding to the first minimum in the radial distribution function of the ionic pair Th^{4+}-F^-. Figure 4 shows the evolution of the main anionic species in the melt: $[ThF_7]^{3-}$, $[ThF_8]^{4-}$ and $[ThF_9]^{5-}$. $[ThF_8]^{4-}$ complex is always

predominant for all the compositions, although on the eutectic composition (22.5 % mol. ThF_4), a light decrease of the 8-fold coordinated complexes in favor of an increase of the 7-fold coordinated complexes in observed, while the amount of $[ThF_9]^{5-}$ remains more or less constant over the entire ThF_4 range, except around the eutectic composition. Content of $[ThF_9]^{5-}$ complexes rises up to 30 mol. % of ThF_4. Near this composition the corresponding Li_3ThF_7 solid is characterized by anionic layers of monocapped antiprisms $[ThF_9]$, compensated by interlayer monocations of Li [40]. This could explain the more important stability of $[ThF_9]^{5-}$ near the eutectic point.

The coordination number varies around 8, as in the crystal [41] when ThF_4 is associated with LiF (Table 4). As the size of the alkaline ion increases (Li → Na → K), analysis of the atomic trajectories derived from MD calculations shows that the average Th-F distance decreases as well as the average coordination number (Figure 5), depending on the temperature and size of the alkali. The same behavior was already observed with AF-ZrF_4 molten mixtures (A^+ = Li^+, Na^+, and K^+) [42].

With KF, coordination varies around 7.1 at 800°C for 25 mol. % ThF_4 up to 8 for the highest contents in ThF_4. Assuming that the variation in thorium coordination with temperature is linear, the extrapolated values at 700°C vary from 7.25 to 7.8 between 25 and 46 % mol. % of ThF_4. These values are in accordance with those calculated by Guo et al. [25].

The comparison between ZrF_4-LiF and ThF_4-LiF systems (Figure 6), at 20°C above the melting point and at the same composition range in ThF_4, shows that the average zirconium environment (7 F^-) is different from thorium one (8 F^-) in the molten state, whereas the two tetravalent ions have the same coordination in the solid state (8 F^-). This difference was already evidenced by Numakura *et al.* [43] and attributed to the difference of ionic radii of both cations (r_{Th} =1.05 Å and r_{Zr}=0.84 Å [44] for a coordination number of 8).

By studying the local environment of fluoride ions, for low ThF_4 contents, the population of free fluorides is very large (65 %) as presented in Figure 7 and decreases very sharply with ThF_4 content increase. As ThF_4 is added, the fluoride ions gradually connect to only one thorium (F-Th) to form isolated anionic complexes $[ThFx]^{4-X}$. From 22.5 % mol. ThF_4 (eutectic composition), the population of fluorine ions connected to only one thorium ion (F-Th) decreases as the proportion of fluoride ions connecting two thorium (Th-F-Th) increases with the amount of ThF_4. From 30-35 mol. % of ThF_4, the presence of fluorine ions connected to three thorium ions is detected. These “triclusters” were already observed in the case of liquid oxides, in particular molten tectosilicates [45]. Their presence has important implications in phase equilibria, mechanisms of viscous flow, and solubility of elements in the

aluminosilicate melts. In our case, the evolution of the different bonds between fluorine and thorium ions can be interpreted as a progressive interconnection between the $[ThF_x]^{4-X}$ species to form a network of Th_xF_y chains. This is consistent with the viscosity increase observed by various measurements and calculations [9, 20, 46-48] when adding tetravalent cations like Th^{4+} in the molten phase of ThF_4-LiF system.

3.2 Molten LiF-UF_4 systems

To complete this study, EXAFS measurements were carried out on molten LiF-UF_4 mixtures at the L_3 edge of uranium. Spectra were collected for several compositions from 5 to 30 mol. % of UF_4 at 20°C above the melting temperature. Figure 8 reports the comparison between experimental and calculated EXAFS signals for sample containing only 5 mol. % of UF_4, close to the one added to LiF-ThF_4 fuel in MSFR.

EXAFS oscillations were calculated at 1175K by using atomic configurations extracted from MD trajectories, to supply input data to FEFF simulation code [36]. As in the case of thorium, the total signal is well reproduced by the sum of three contributions weighted by the proportion of each uranium-based species found in the molten phase (Figure 8). For this composition at 1175K, 59 % of $[UF_8]^{4-}$, 30% of $[UF_9]^{5-}$ and 9 % of $[UF_7]^{3-}$ with mean U-F distances of 2.30 Å, 2.38 Å and 2.24 Å respectively are obtained. The results for other compositions are gathered in Table 5. Whatever the compositions, following the example of LiF-ThF_4 system, the 8-fold coordinated $[UF_8]^{4-}$ complexes are predominantly present in the liquid phase.

With a slightly smaller ionic radius than thorium (r_{U4+}=1 Å), the uranium ion is also less surrounded by fluoride ions over the entire composition range studied, as shown in the Figure 9. For these two cations, the CN remains generally constant by oscillating around an average value as function of the composition (7.8 and 8.02 for U^{4+} and Th^{4+} respectively), close to 8 as for solid compounds and higher than the value calculated in the case of Zr^{4+} for the LiF-ZrF_4 system for the low cation contents (< 22 mol. %) [30].

This singular behavior of zirconium ions compared to U^{4+} and Th^{4+} cations is also noticeable in the computations from MD simulations of the number of bridging fluoride ions (Figure 10) between anionic complexes with addition of MF_4 (M = Zr^{4+}, Th^{4+}, U^{4+}). This average number includes both free fluorine (not connected to any cation), fluorine ions connected to 1 cation (F-M, M=U^{4+}, Th^{4+}, Zr^{4+}) or fluorine ions connected to 2 cations (M-F-

M).The procedure to calculate this number is described in a previous work [30]. For each fluorine ion examined, we use geometrical criteria defined from the first minimum of the radial distribution function of the F-M (M=U^{4+}, Th^{4+}, Zr^{4+}) and M-M pairs respectively. To determine the type of fluorine ion we are dealing with, the method consists in first testing the distance between the F ion considered and the M cations located around it, then the distance between the M - M cations. If these distances are less than the criteria we have set ourselves, we can then determine whether the fluorine ion is free, connected to one cation or two M cations. For the three cations, the evolution of this number is monotonous and nonlinear with composition as expected. However, the curve for ZrF_4 moves away gradually from those obtained for ThF_4 and UF_4, in particular from 20 mol. %, and aims towards 1.2 for 40 mol. %. This discrepancy suggests that it is easier to obtain a liquid partly associated with addition of UF_4 or ThF_4 more than ZrF_4. It is coherent with the simulations and experimental data for viscosity as function of composition.

This number of bridging fluoride ions represents an average situation which takes into account the free fluorine ions (F^-), the F^- involved in isolated M-based (M = Zr^{4+}, Th^{4+}, U^{4+}) complexes $[MF_x]^{4-x}$ and the F^- connecting the complexes together. The amount of free F^- is more important in the case of zirconium system. This excess of F^- acceptors leads to an increase of the basicity of the molten LiF-ZrF_4 mixtures [49] relative to the thorium or uranium fluoride salts (Figure 11a). Whatever the type of cations, the rate of the free fluorine decreases monotonously up to 30 mol. %. Then, all the fluorine ions are connected to a cation, contributing to an increase of the melt viscosity. Depending on the tetravalent ion, the connections between the anionic complexes $[MF_x]^{4-x}$ are different. In ZrF_4 system, the fluorine ions are mostly involved in Zr-F bonds to form Zr-based complexes (Figure 11b). Up to 30 mol. %, these complexes are weakly linked between them (Figure 11c), contrary to ThF_4 and UF_4 mixtures where the anionic species are bound from 20 mol. %. At equivalent concentration, the viscosity in these mixtures should be more important than in the molten LiF-ZrF_4 system. For the binary systems LiF-ThF_4 and LiF-UF_4, we find that the amount of fluorine ions linked to two cations M (M=U^{4+}, Th^{4+}) is greater than in the case of the LiF-ZrF_4 system. Moreover, we observe that the proportion of $(MF_X)^{4-X}$ (M=Th^{4+}, U^{4+}) complexes connected by fluorine ions increases with the addition of MF_4.
This is consistent with the formation of $(Th_xF_y)^{4x-y}$ or $(U_xF_y)^{4x-y}$ chains in the liquid phase instead of isolated anionic complexes $(ThF_X)^{4-x}$ or $(UF_X)^{4-x}$. This structuring of the liquid leads to a slowing down of the ionic mobility in these systems and thus to an increase in the viscosity in these molten mixtures.

3.3 Molten [LiF-ThF4]eutectic + x mol. % UF_4

The previous results indicate that LiF-ThF_4 and LiF-UF_4 binaries systems have the same behavior depending on the composition. The question is what would happen if a few mole percent of UF_4 is added in a molten salt LiF-ThF_4?

Eutectic composition 77.5 mol. % LiF - 22.5 mol. % ThF_4 with 4 mol. % of UF_4 was investigated. Although this composition is the one considered for the operation of future molten salt reactors, the study was extended to other compounds around this key concentration. The results are reported in Table 6. Figure 12 shows the EXAFS oscillations calculated and recorded at the threshold L3 of thorium for a temperature of 700°C for the sample with 4 mol. % of UF_4 at LiF-ThF_4 eutectic composition. Except for the peak of double excitation situated at 10 $Å^{-1}$), a very good agreement between the experimental and calculated EXAFS signals can be noted. No significant changes in the EXAFS spectra depending on the amount of UF_4 added was noticed. This was confirmed by the evolution of thorium average coordination number as a function of UF_4 proportion (Figure 13) calculated from the statistical analysis of ionic trajectories recorded during the molecular dynamic simulations of the liquid. This number increases very slightly (less than 1 %) but remains very close to 8 fluorine neighbors. The average coordination number does not seem to be affected by addition of UF_4. $[ThF_8]^{-4}$ complexes are still the major species in spite of a slight redistribution across $[ThF_7]^{-3}$ and $[ThF_9]^{-5}$ species when UF_4 evolves towards higher concentrations (Figure 14).

By contrast, the impact of UF_4 addition with only 4 mol. % UF_4 added, involve some decrease of the percentage of anionic species $(Th_XF_y)^{4X-Y}$ by 50% and increase of the population $(Th_XU_yF_Z)^{4X+4Y-Z}$ from 0% to 8%. (Figure 15).

A more detailed analysis of the links between fluorine ions and thorium and/or uranium ions, shows (Figure 16a) a slight increase in the population of free fluorine ions and a decrease in the proportion of $[Th_XF_Y]^{4X-Y}$ species when UF_4 is added to LiF-ThF_4 (eutectics). Although these $[Th_XF_Y]^{4X-Y}$ species are in the majority whatever the UF_4 content, the presence of uranium ions also leads to the formation of some isolated $[UF_X]^{4-X}$ complexes (X = 6, 7, 8 for an average value between 7.3 and 7.1 fluorine ions around the uranium ions) and $[Th_XU_YF_Z]^{4(X+Y)-Z}$ chains which increase with molar percentage of UF_4. No $[U_2F_X]^{8-X}$ "dimers" were observed. In $[Th_XF_Y]^{4X-Y}$ category, it is mainly observed (Figure 16b) that quantity of $[ThF_X]^{4-X}$ monomers (X = 6, 7, 8, 9 with a mean value of 7.5 to 7.4 fluorine ions around thorium ions in the studied range of UF_4) decreases as soon as UF_4 is added before stabilizing at 2 mol. % of UF_4, while $[Th_2F_X]^{8-X}$ "dimers" and $[Th_3F_X]^{12-X}$ "trimers" continue to decline. Then, the percentage of $[UF_X]^{4-X}$ complexes increases slightly with UF_4 content and proportion of $[Th_XU_YF_Z]^{4(X+Y)-Z}$ complexes rises very strongly at the same time: uranium

ion acts as a "network builder" by connecting the $[Th_XF_Y]^{4X-Y}$ chains together, thus causing the release of excess fluorine ions following the rearrangement of these anionic species. Indeed, from Figure 16b, addition of uranium to the mixture in the form of UF_4 mainly promotes the connection of $[Th_XF_Y]^{4X-Y}$ species between them to form $[Th_XU_YF_Z]^{4(X+Y)-Z}$ anionic complexes.

To give a better picture of this situation, the Figure 17 presents a visualization of one snapshot extracted from the ionic trajectory calculated by molecular dynamic simulations at 700°C for the eutectic composition of the [LiF-ThF_4] system with 4 mol. % of UF_4. Lithium atoms were purposely omitted for a better observation of the formation of polyhedral chains $[ThF_4]^{4-X}$ (green) on which the $[UF_4]^{4-X}$ species (blue) thus releasing fluorine ions (yellow). The average lengths of Th-F and U-F bonds are 3.07 Å and 3.17 Å, respectively.

Finally, reporting the F- / ($[Th_XF_Y]^{4X-Y}$ + $[Th_XU_YF_Z]^{4(X+Y)-Z}$) ratio as a function of the UF_4 content (Figure 18), an initial increase and a stabilization from 2 mol. % of UF_4 are observed. Additional contribution of free fluorine by addition of UF_4 in the LiF-ThF_4 mixture tends to increase [49-50] the basicity and reduce its viscosity as shown in Figure 19. The viscosities of the simulated systems were determined by integrating the autocorrelation function of the stress tensor calculated during the MD simulations [51].

4. Conclusion

The local structure around the tetravalent cations M^{4+} in the AF-MF_4 (A= Li^+, Na^+, K^+; M=Th^{4+}, U^{4+}) and [77.5 mol. % LiF- 22.5 mol. % ThF_4] + x mol. % UF_4 (x=1, 2, 3, 4) molten systems by combining high temperature EXAFS experiments and classical molecular dynamics simulations was examined.

Whatever the cation studied (M=Th^{4+}, U^{4+}), the presence of free fluorine ions coexisting with $[MF_8]^{4-}$, $[MF_7]^{3-}$ and $[MF_9]^{5-}$ anionic complexes in the liquid phase was confirmed. Depending MF_4content, these species are isolated or connected together by fluorine ions to form $(Th_xF_y)^{4x-y}$ long chains. Formation of such a network leads to an increase of viscosity in these systems.

For constant temperatures or 20°C higher than the melting point, the species distribution is changed according to the composition and cation considered. However, $[MF_8]^{4-}$ species remain predominant over the entire range of compositions studied. In the case of molten LiF-ThF_4 and LiF-UF_4, the average number of F^- neighbors around Th^{4+} and U^{4+} tetravalent cations (8.0 and 7.8 respectively) is relatively stable up to 35 mol. % of

MF_4. These values are close to those determined in the solid phase, unlike the one found in the system LiF-ZrF_4 was determined to be 6.8 in the same composition range. As with the zirconium system, when the size of A^+ alkaline ion (A^+=Li, Na and K) increases, a decrease in the average coordination of actinide ions is observed toward a value around 7 instead of 6.1 like in the AF-ZrF_4 system.

For the three cations, the number of bridging fluorine ions between complexes rises monotonically with the mole fraction of MF_4, but this enhancement is less important in the case of ZrF_4. For low concentration, the free fluorine ions content predominates and for high contents (>10 mol. %), fluorine ions are involved in the coordination of complexes. For larger MF_4 quantities, more bonds are formed between complexes $[MF_x]^{4-x}$ thanks to bridging fluorine ions. These connections only start to increase from 35 mol. % for LiF-ZrF4 mixtures and from 10 mol. %. with ThF_4 and UF_4.

The tendency to form a highly structured liquid in the LiF-ThF_4 system can be slowed down by adding a few moles of UF_4 to the mixture. The addition of uranium has very little effect on the distribution of complexes $[ThF_X]^{4-x}$. On the contrary, it leads to a slight increase in the number of free fluorine ions due to the rupture of the Th-F-Th chains to form complexes $[UF_x]^{4-x}$ isolated or connected to the $(Th_xF_y)^{4x-y}$ chains. This rearrangement of the structure of the liquid results in a slight decrease in viscosity and an increase in the basicity of the mixtures depending on the amount of UF_4 added.

ACKNOWLEDGEMENTS

The authors acknowledge the French program NEEDS and the regional Council of the region Centre - Val de Loire for their financial support. The EXAFS measurements were obtained as part of experimental projects (N°: 2014G182 and N°: 2015G154) performed on the synchrotron facilities of KeK (beamline BL27B of the Photon Factory, Tsukuba- Japan). The molecular dynamics calculations were carried out with the computer resources of the "Centre de Calcul Scientifique en region Centre" (Orléans, France) and those of the CEMHTI laboratory for data analysis, thanks to the technical support provided by the engineers in charge of these facilities L. Catherine and F. Vivet respectively.

ABBREVIATIONS

EXAFS: Extended of X-Ray absorption of the fine structure; MD: molecular dynamic

BIBLIOGRAPHY

1. **O. Benes, R. J. M. Konings.** Molten Salt Reactor Fuel and Coolant. *Comprehensive Nuclear Materials.* 2012, Vol. 3, 359-389.

2. **P. N. Haubenreich, J. R. Engel.** Experience with the Molten-Salt Reactor Experiment. *Nuclear Applications and Technology.* 1970, Vol. 8:2, 118-136.

3. **S. Delpech, E. Merle-Lucotte, D. Heuer, M. Allibert, V. Ghetta, C. Le-Brun, X. Doligez, G. Picard.** *Journal of Fluorine Chemistry.* 2009, Vol. 130, 11.

4. **J. Serp, M. Allibert, O. Benes, S. Delpech, O. Feynberg, V. Ghetta, D. Heuer, D. Holcomb, V. Ignatiev, J. L. Kloosterman, L. Luzzi, E. Merle-Lucotte, J. Uhlir, R. Yoshioka, D. Zhimin.** *Progress in Nuclear Energy.* 2014, Vol. 77, 308-319.

5. **E. Capelli, O. Benes, J. Y. Colle, R. J. M. Konings.** *Physical Chemistry Chemical Physics.* 2015, Vol. 17, 30110-30118.

6. **D. Hill, S. Cantor, W. Ward.** *Journal of Inorganic and Nuclear Chemistry.* 1967, Vol. 29, 241-243.

7. **J. Senegas, S. Pulcinelli.** *Journal of Fluorine Chemistry.* 1988, Vol. 38, 375-389.

8. **E. Brown, B. Porter.** *Electrical conductivity and density of molten systems of uranium tetrafluoride and thorium fluoride with alkali fluorides.* Reno Metallurgy Research Center, Nevada : Bureau of Mines, 1963. OSTI ID: 4049148 / BM-RI-6500 / NSA-18-035492.

9. **Y. F. Chervinskii, V. N. Desyatnik, A. I. Nechaev.** *Zhurnal Fizicheskoi Khimi.* 1982, Vol. 56, 1946-1949.

10. **C. Hamel, P. Chamelot, A. Laplace, E. Walle, O. Dugne, P. Taxil.** *Electrochimica Acta.* 2007, Vol. 52, 3995.

11. **P. Taxil, L. Massot, C. Nourry, M. Gibilaro, P. Chamelot, L. Cassayre.** *Journal of Fluorine Chemistry.* 2009, Vol. 130, 94.

12. **H. Groult, A. Barhoun, H. el Ghallali, S. Borensztjan, F. Lanthelme.** *Journal of Electrochemical Society.* 2008, Vol. 155, E19.

13. **O. Conocar, N. Douyere, J. Lacquement.** *Journal of Nuclear Materials.* 2005, Vol. 344, 136-141.

14. **V. Dracopoulos, J. Vagelatos, G. N. Papatheodorou.** *Journal Chemical Society Dalton Transactions.* 2001, 1117.

15. **L. M. Toth, G. E. Boyd.** *Journal of Physical Chemistry.* 1973, Vol. 77, 2654.

16. **C. Bessada, D. Zanghi, O. Pauvert, L. Maksoud, A. Gil-Martin, V. Sarou-Kanian, P. Melin, S. brassamin, A. Nezu, H. Matsuura.** *Journal of Nuclear Materials.* 2017, Vol. 494, 192-199.

17. **A. L. Smith, M. N. Verleg, J. V. Vlieland, D. de Haas, J. A. Ocadiz-Florès, P. A. Martin, J. Rothe, K. Dardenne, M. Salanne, A. E. Gheribi, E. Capelli, L. van Eijck, J. M. Konings.** *Journal of Synchrotron Radiation.* 2019, Vol. 26, 124-136.

18. **J. Sun, X. Guo, J. Zhou, J. Dai, S. Song, H. Bao, J. Lin, H. Yu, S. He, F. Jiang, D. Long, L. Zhang and J.-Q. Wang.** *Journal of Synchrotron Radiation.* 2019, Vol. 26, 1733-1741.

19. **J. Dai, D. Long, P. Huai, Q. Li.** *Journal of Molecular Liquids.* 2015, Vol. 211, 747-753.

20. **L. C. Dewan, C. Simon, P. A. Madden, L. W. Hobbs, M. Salanne.** *Journal of Nuclear Materials.* 2013, Vol. 434, 322.

21. **F. Hutchinson, M. Wilson, P. A. Madden.** *Molecular Physics.* 2001, Vol. 99, 811.

22. **P. A. Madden, M. Wilson.** *Chemical Society Reviews.* 1996, Vol. 25, 339.

23. **A. E. Gheribi, D. Corradini, L. C. Dewan, P. Chartrand, C. Simon, P. A. Madden, M. Salanne.** *Molecular Physics.* 2014, Vol. 112, 1306-1312.

24. **J. B. Liu, X. Chen, Y. H. Qiu, C. F. Xu, W. H. Eugen Schwarz, J. Li.** *Journal of Physical Chemistry B.* 2014, Vol. 118, 13954-13962.

25. **X. Guo, H. Q. Qian, Hongliang, J. Dai, W. L. Liu, J. Hu, R. Shen and J. Wang.** *Journal of Molecular Liquids.* 2019, Vol. 277, 409-417.

26. **A. L. Rollet, C. Bessada, Y. Auger, P. Auger, P. Melin, M. Gailhanou, D. Thiaudière.** *Nuclear Instruments and methods in Physics Research B.* 2004, Vol. 226, 447.

27. **C. Bessada, A.-L. Rollet, D. Zanghi, P. Melin, E. Labrude, S. Brassamin, O. Pauvert, C. Thefany.** *Speciation, techniques and facilities for radiactive materials at synchrotron light sources.* 2009, Vol. © OECD/NEA, 117-122.

28. **H. Konishi, A. Yokoya, H. Shiwaku, H. Motohashi, T. Makita, Y. Kashihara, S. Hashimoto, T. Harami, T. Sasaki, H. Maeta et al.** *Nuclear Instruments and Methods in physics research A.* 1996, Vol. 372, 322.

29. **M. Newville.** *Journal of Synchrotron Radiation.* 2001, Vol. 8, 322.

30. **O. Pauvert, D. Zanghi, M. Salanne, C. Simon, A. Rakhmatullin, H.Matsuura, Y.Okamoto, F. Vivet, C. Bessada.** *Journal of Physical Chemistry B.* 2010, Vol. 114, 6472-6479.

31. **M. Salanne, C. Simon, P. Turq, R. J. Heaton, P. A. Madden.** *Journal of Physical Chemistry B.* 2006, Vol. 110, 11461-11467.

32. **M. Salanne, C. Simon, P. Turq, P. A. Madden.** *Journal of Fluorine Chemistry.* 2009, Vol. 130, 38-44.

33. **M. Salanne, C. Simon, P. Turq, P. A. Madden.** *Journal of Physical Chemistry B.* 2008, Vol. 112, 1177.

34. **M. Salanne, B. Rotenberg, S. Jahn, R. Vuilleumier, C. Simon, P. A. Madden.** *Theoritica Chimica Acta.* 2012, Vol. 131, 1-16.

35. **L. C Dewan.** *Thesis of Massachusetts Institute of Technology.* 2013.

36. **A. Ankudinov, B. Ravel, J. Rehr, S. Conradson.** *Physical Review B.* 1998, Vol. 58, 007565.

37. **W. H Zachariasen.** *Journal of American Society.* 1948, Vol. 70, 2147.

38. **Y. Okamoto.** *Nuclear Instrument and Methods in physics research A.* 2004, Vol. 526, 572.

39. **C. Hennig.** *Physical Review B.* 2007, Vol. 75, 35120.

40. **S. H. Pulcinelli, R. H. Santos, J. Senegas.** *Journal of Fluorine Chemistry.* 1989, Vol. 42, 41-50.

41. **M. S. Wickleder, B. Fourest, P. K. Dorhout.** *Thorium in the chemistry of the actinide and Transactinide Elements.* New-York : Springer, 2006. Morss L. R, Edelstein N. M., Fuger J. Eds.

42. **O. Pauvert, M. Salanne, D. Zanghi, C. Simon, S. Reguer, D. Thiaudière, Y. Okamoto, H. Matsuura, C. Bessada.** *Journal of Physical Chemistry B.* 2011, Vol. 115, 9160-9167.

43. **M. Numakura, N. Sato, C. Bessada, Y. Okamoto, H. Akatsuka, A. Nezu, Y. Shimohara, K. Tajima, H. Kawano, T. Nakahagi, H. Matsuura.** *Progress in Nuclear.* 2011, Vol. 53, 994.

44. **D. Shannon.** *Acta Crystallographica Section A .* 1976, Vol. 32, 751.

45. **M. J. Toplis, D. B. Dingwell, T. Lenci.** *Geochimica et Cosmochimica acta.* 1997, Vol. 61, 2605-2612.

46. **S. Cantor.** *Density and Viscosity of Several molten Fluoride Mixtures.* Oak Ridge, USA, 1973. ORNL/TM-4308.

47. **V. Khokhlov, V. Ignatiev, V. Afonichkin.** *Journal of Fluorine Chemistry .* 2009, Vol. 130, 30-37.

48. **A. V. Merzlyakov, V. V. Ignatiev, S. S. Abalin.** *Journal of Nuclear Materials.* 2011, Vol. 419, 361.

49. **M. Kergoat, L. Massot, M. Gibilaro, P. Chamelot.** *Electrochimica Acta.* 2014, Vol. 120, 258-263.

50. **D. Williams, L. Toth, K. Clarno.** *Assessment of candidate Molten salt coolants for the Advanced High-Temperature Reactor (AHTR).* Oak Ridge, 2006. ORNL/TM-2006/12.

51. **N. Ohtori, M. Salanne and P. A. Madden.** *Journal of Chemical Physics.* 2009, Vol. 130, 104507.

Table captions

Table 1: Conditions used for molecular dynamics simulations on the LiF-ThF_4 system.

Table 2: Conditions used for molecular dynamics simulations on the LiF-UF_4 system.

Table 3: Conditions used for molecular dynamics simulations on the $[LiF\text{-}ThF_4]_{eut}$ (22.5 mol. % - 77.5 mol. %) + x mol. % UF_4 (x=1, 2, 3, 4) system at 975K.

Table 4: Anionic percentage for each ionic polyhedra $[ThF_x]^{4-x}$ formed in LiF-ThF_4 system as function of temperature and composition.

Table 5: Anionic percentage and distances (U^{4+}-F^-) for each ionic polyhedra $[UF_x]^{4-x}$ formed in LiF-UF_4 system as function of temperature and composition. The average coordination of U and average distance U-F were deduced of calculations carried out on 27000 clusters of U^{4+} ions surrounded of fluorine neighbours.

Table 6: Percentage of Th^{4+} and U^{4+} coordination numbers as a function of UF_4 content in the $[ThF_4\text{-}LiF]_{eut}$ (22.5 mol. % - 77.5 mol. %) + x mol. % UF_4 (x=1, 2, 3, 4) system at 970K.

mol. % ThF_4	N_{F-}	N_{Th4+}	N_{Li+}	T (K)	Volume ($Å^3$)	Density (g/cm^3)
5	299	13	247	1115	7043	2.45
10	312	24	216	1070	7066	3.05
15	329	34	193	1015	7211	3.57
18	325	38	173	970	6992	3.84
20	240	30	120	970	5132	4.00
23	316	43	144	855	6550	4.30
25	350	50	150	875 / 970	7244 / 7439	4.42 / 4.31
30	361	57	133	855 / 970	7312 / 7619	4.75 / 4.58
35	370	63	118	970	7770	4.82
40	380	69	104	1035	8093	4.92
50	395	79	79	1135	8604	5.09

Table 1

mol. % UF_4	N_{F-}	N_{U4+}	N_{Li+}	T (K)	Volume ($Å^3$)	Density (g/cm^3)
5	299	13	247	1175	7145	2.44
10	312	24	216	1125	7210	3.41
15	329	34	193	1075	7194	3.63
20	344	43	172	1000	7272	4.1
27.4	359	54	143	825 / 875 /925 / 975	7185 /7273 / 7295 / 7415	4.76 / 4.7 / 4.69 / 4.62
30	361	57	133	875	7237	4.89

Table 2

mol. % UF_4	N_{F-}	N_{Th4+}	N_{U4+}	N_{Li+}	Volume ($Å^3$)	Density (g/cm^3)
0	335	45	0	155	7156	4.15
1	316	41	2	143	6718	4.20
2	319	41	4	141	6677	4.35
3	321	40	6	138	6764	4.36
4	324	40	7	136	6817	4.39

Table 3

mol % ThF_4	T(K)	Anionic Fraction of $[ThF_x]^{4-x}$ (%)					Average CN
		6	7	8	9	10	
5	1115	0.28	18.63	62.71	17.98	0.39	8.00
10	1070	0.40	18.11	63.91	17.15	0.41	7.99
15	1015	0.38	17.83	62.11	19.08	0.58	8.02
18	970	0.29	16.67	61.63	20.68	0.72	8.05
20	970	0.61	20.73	61.97	16.29	0.40	7.95
23	855	0.15	13.63	62.55	22.86	0.80	8.10
25	875	0.32	15.06	60.20	23.42	0.98	8.09
	970	0.78	22.39	59.19	17.02	0.62	7.94
30	855	0.27	12.18	56.51	29.14	1.87	8.20
	970	0.74	20.37	55.55	22.06	1.26	8.03
35	970	0.82	19.06	54.66	23.71	1.72	8.06
40	1035	1.5474	22.78	52.97	21.26	1.42	7.98
50	1135	2.57	28.05	49.78	18.094	1.45	7.87

Table 4

Mol. % UF_4	T(K)	% Anionic Fraction of $[UF_x]^{4-x}$ (%) d_{U-F}(Å)					Average
		6	7	8	9	10	CN d_{U-F} (Å)
5	1175	1.27	30.55	59.37	8.71	0.1	7.75
		2.17	2.24	2.30	2.38	2.45	2.29
10	1125	2.01	34.59	55.96	7.35	0.09	7.68
		2.18	2.24	2.30	2.37	2.44	2.28
15	1075	1.14	27.27	59.59	11.74	0.26	7.82
		2.17	2.24	2.30	2.37	2.46	2.29
20	1000	1.10	26.96	59.51	12.13	0.29	7.86
		2.17	2.23	2.30	2.37	2.45	2.29
27.4	825	0.75	21.65	62.78	14.54	0.29	7.90
		2.17	2.23	2.29	2.35	2.42	2.29
	875	0.92	21.43	60.44	16.71	0.50	7.91
		2.17	2.23	2.29	2.36	2.43	2.29
	925	1.08	24.66	58.90	14.93	0.43	7.85
		2.17	2.23	2.30	2.36	2.43	2.29
	975	1.54	27.36	56.64	14.04	0.41	7.86
		2.17	2.24	2.30	2.37	2.44	2.29
30	875	0.98	22.39	59.29	16.55	0.50	7.89
		2.17	2.23	2.30	2.36	2.43	2.29

Table 5

mol. % UF_4	% Th^{4+} coordination number (CN)					Avg.	% U^{4+} coordination number (CN)					Avg.
	6	7	8	9	10	CN / d_{Th-F}(Å)	6	7	8	9	10	CN / d_{U-F}(Å)
0	0.63	19.34	59.89	19.38	0.75	8.00 / 2.349	-	-	-	-	-	-
1	0.53	17.99	58.99	21.43	1.05	8.05 / 2.354	1.04	26.87	59.57	12.26	0.27	7.84 / 2.290
2	0.43	15.98	58.55	23.78	1.24	8.09 / 2.358	1.16	24.76	59.39	14.40	0.30	7.88 / 2.291
3	0.60	18.54	58.59	21.24	1.02	8.04 / 2.354	1.28	24.42	57.53	16.33	0.45	7.90 / 2.294
4	0.51	17.35	57.62	23.14	1.36	8.08 / 2.358	1.26	24.63	58.18	15.40	0.53	7.89 / 2.294

Table 6

Figure captions

Figure 1: Fourier transform of the EXAFS signals recorded at room temperature and 975 K for 75 mol. % LiF -25 mol.% ThF4 composition.

Figure 2: Comparison between the calculated oscillations and the experimental EXAFS curves (Th -L_{III}) of three studied compositions (82%LiF-18%ThF_4, 75%LiF-25%ThF_4, 65%LiF-35%ThF_4) in the liquid phase at high temperature (700°C).

Figure 3: Calculated Th L_{III}-edge EXAFS function k^2 $\chi(k)$ of LiF-ThF_4 (25 mol.% - 75 mol.%).

Figure 4: Evolution of the percentages of the different Th-based complexes coexisting in the melts in the molten LiF-ThF_4 system, from 0 to 100 mol. % ThF_4 at 20°C above the melting temperature.

Figure 5: a) Mean coordination of thorium and b) average distance (Th-F) in the molten ThF_4-AF (A= Li, Na, K) systems for various temperatures.

Figure 6: Average coordination number of thorium and zirconium ions in the LiF-MF_4 (M= Th^{4+}, Zr^{4+}) systems at 20°C above the melting point.

Figure 7: Evolution of the number of connections between F and Th ions in the LiF-ThF_4 system, from 0 to 100 mol. % ThF_4 at 20°C above the melting temperature.

Figure 8: Comparison between the experimental and calculated EXAFS signals (U L_{III}-edge for the sample containing only 5 mol. % of UF_4 in LiF at 900°C. In insert, decomposition of calculated U L_{III}-edge EXAFS function k^2 $\chi(k)$ of LiF-UF_4 (5 mol.% - 95 mol.%) at 1175K.

Figure 9: Average coordination number of the thorium ion, zirconium ion and uranium ion in the LiF -MF_4 (M= U^{4+}, Th^{4+}, Zr^{4+}) systems at 20°C above the melting temperature

Figure 10: Average bridging F/$[MF_4]^{4-x}$ of the thorium ion, zirconium ion and uranium ion in LiF MF_4 (M= U^{4+}, Th^{4+}, Zr^{4+}) systems at 20K above the melting temperature

Figure 11: Bridging F/$[MF_4]^{4-x}$ in the LiF-MF_4 systems (M= U^{4+}, Th^{4+}, Zr^{4+}) at 20K above the melting temperature. a) free fluorine, b) fluorides involved in coordination of one complex (F-Al) and c) fluorides forming bridges between complexes (M-F-M).

Figure 12 Comparison between the experimental and calculated EXAFS signals (Th L_{III}-edge, 700°C) for the sample with 4 mol. % of UF_4 at the eutectic composition of LiF-ThF4 (22.5 mol. % - 77.5 mol. %).

Figure 13: Average coordination number and F bridging in LiF-ThF_4 (22.5 mol. % - 77.5 mol. %) with addition of UF_4 at 700°C.

Figure 14: Evolution of the different Th-based complexes coexisting in the melts in the molten LiF-ThF_4 (22.5 mol. % - 77.5 mol. %) + mol. % UF_4 system, at 700°C.

Figure 15: Distribution of anionic species as a function of the UF_4 content in the molten LiF-ThF_4 (22.5 mol. % - 77.5 mol. %) + mol. % UF_4 system, at 700°C.

Figure 16: Distribution of $[Th_XF_Y]^{4X-Y}$ species (a) and $[Th_XU_YF_Z]^{4(X+Y)-Z}$ (b) according to the molar percentage of UF_4 in the mixture LiF-ThF_4-UF_4 at 700°C.

Figure 17: Atomic configuration extracted from the ionic trajectories calculated by molecular dynamics for the $[ThF_4\text{-}LiF]_{eutectic}$ with 4 mol. % of UF_4 system at 700°C. Lithium ions have been deliberately omitted for a better observation. The average lengths of Th-F and U-F bonds are 3.07 Å and 3.17 Å, respectively.

Figure 18: F- / ($[Th_XF_Y]^{4X-Y}$ + $[Th_XU_YF_Z]^{4(X+Y)-Z}$) ratio as a function of the UF_4 content.

Figure 19: Evolution of the viscosity as function of UF_4 in in the molten LiF-ThF_4 (22.5 mol. % - 77.5 mol. %) at 700°C.

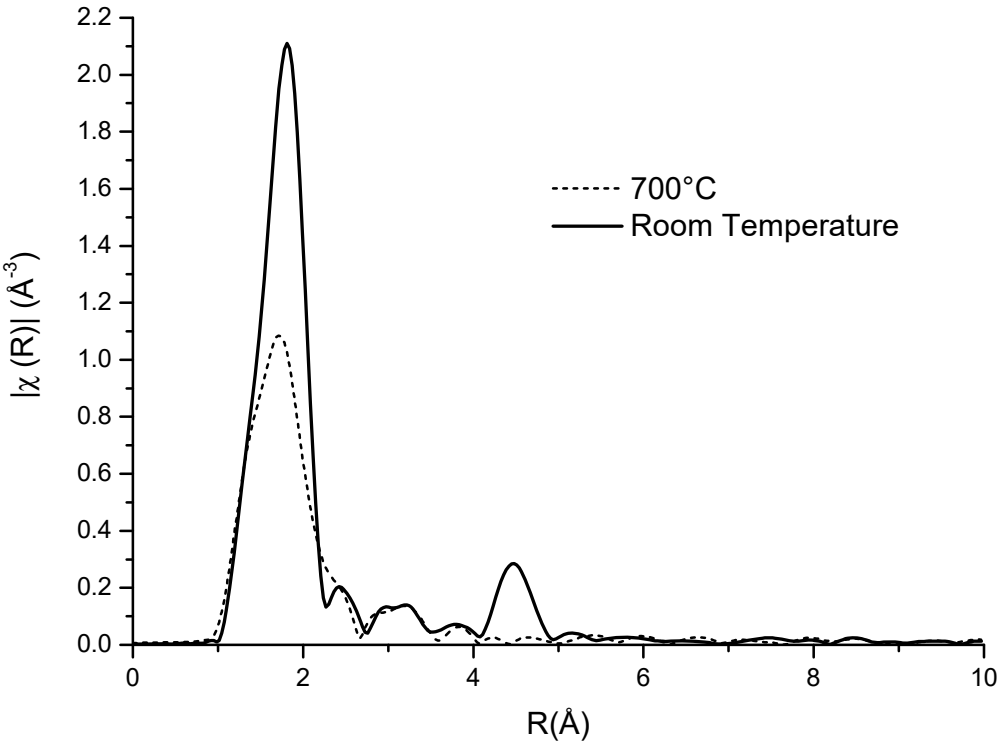
2.2
2.0
1.8
1.6
1.4
1.2
1.0
0.8
0.6
0.4
0.2
0.0
|χ (R)| (Å-3)
0
2
4
6
8
10
R(Å)
700°C
Room Temperature

Figure 1

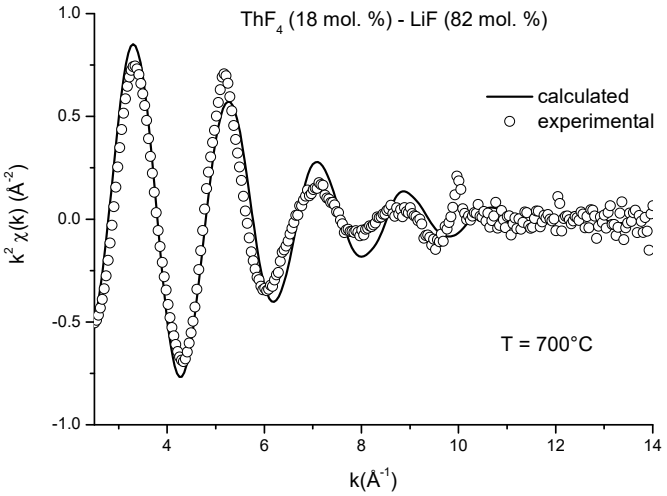
ThF4 (18 mol. %) - LiF (82 mol. %)
calculated
experimental
T = 700°C
k2 χ(k) (Å-2)
k(Å-1)

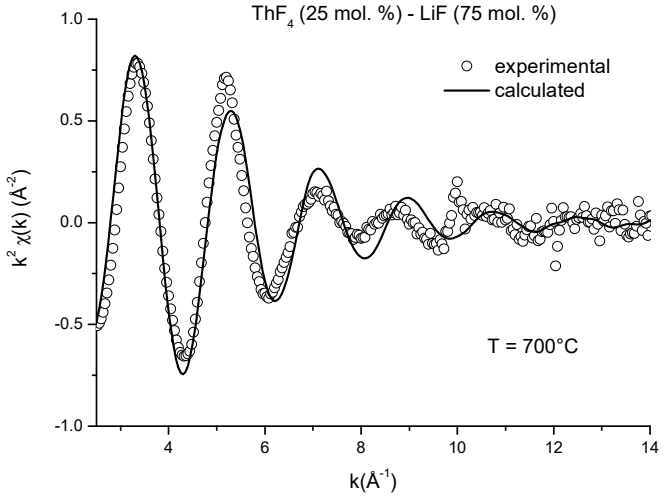
ThF4 (25 mol. %) - LiF (75 mol. %)
experimental
calculated
T = 700°C
k2 χ(k) (Å-2)
k(Å-1)

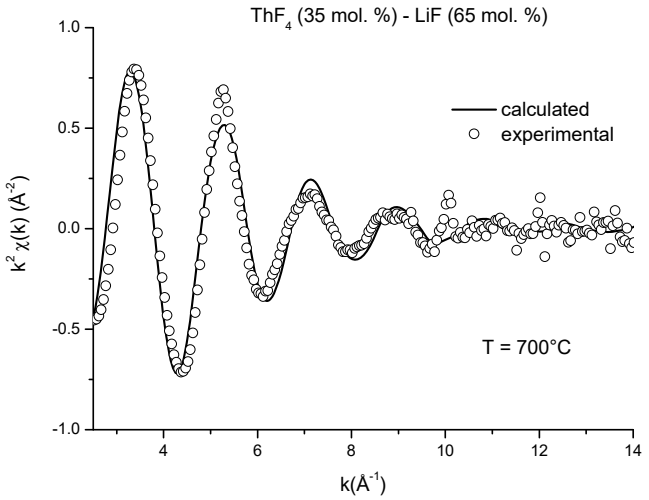
ThF4 (35 mol. %) - LiF (65 mol. %)
calculated
experimental
T = 700°C
k2 χ(k) (Å-2)
k(Å-1)

Figure 2

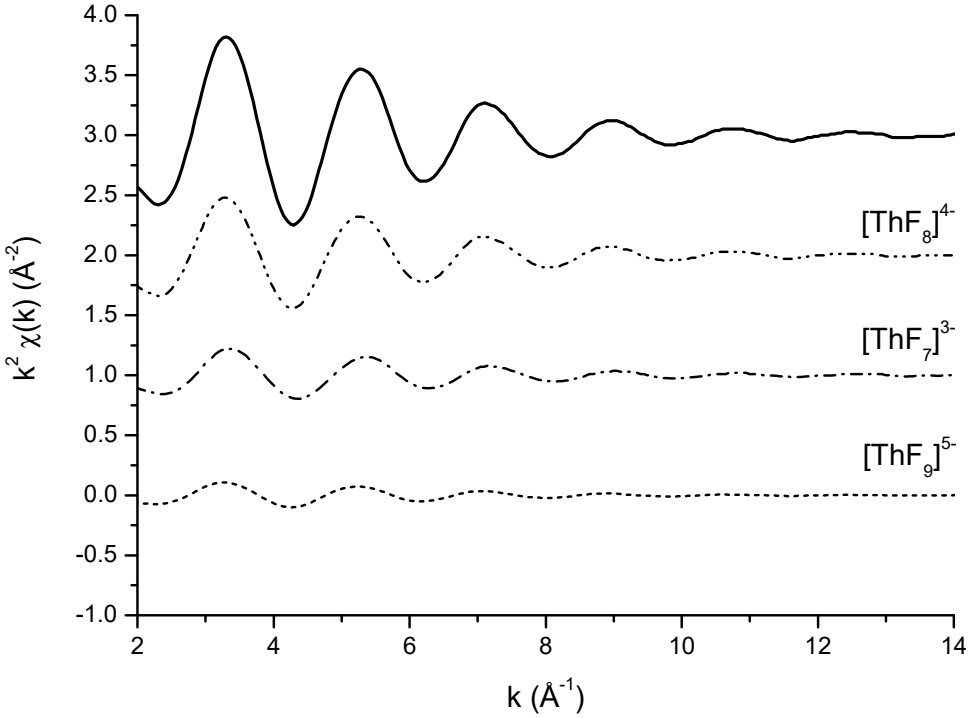

Figure 3

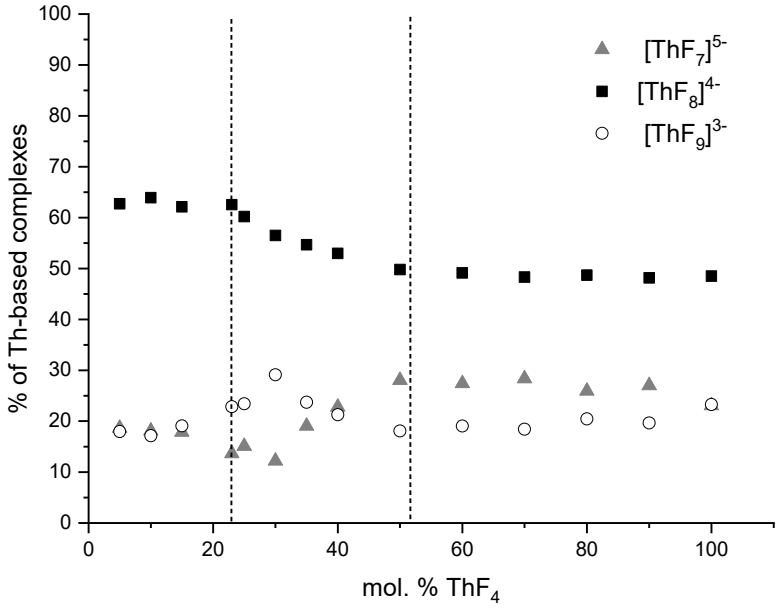

Figure 4

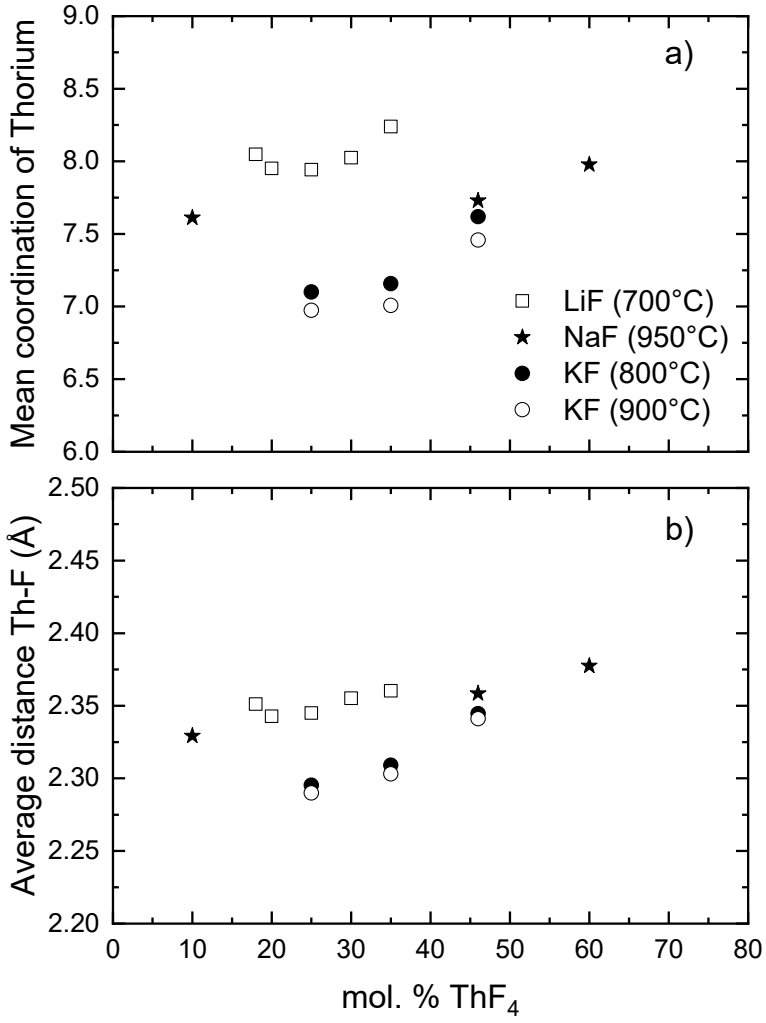

Figure 5

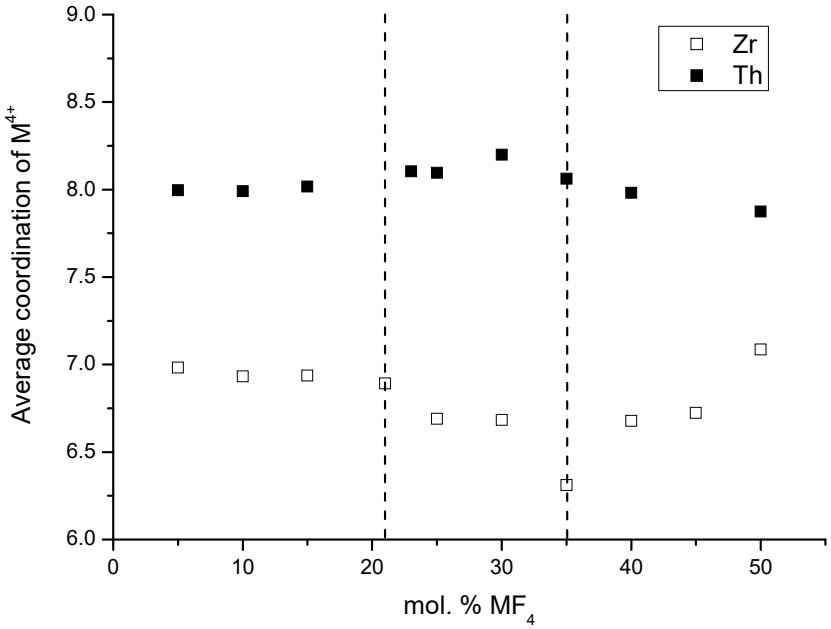

Figure 6

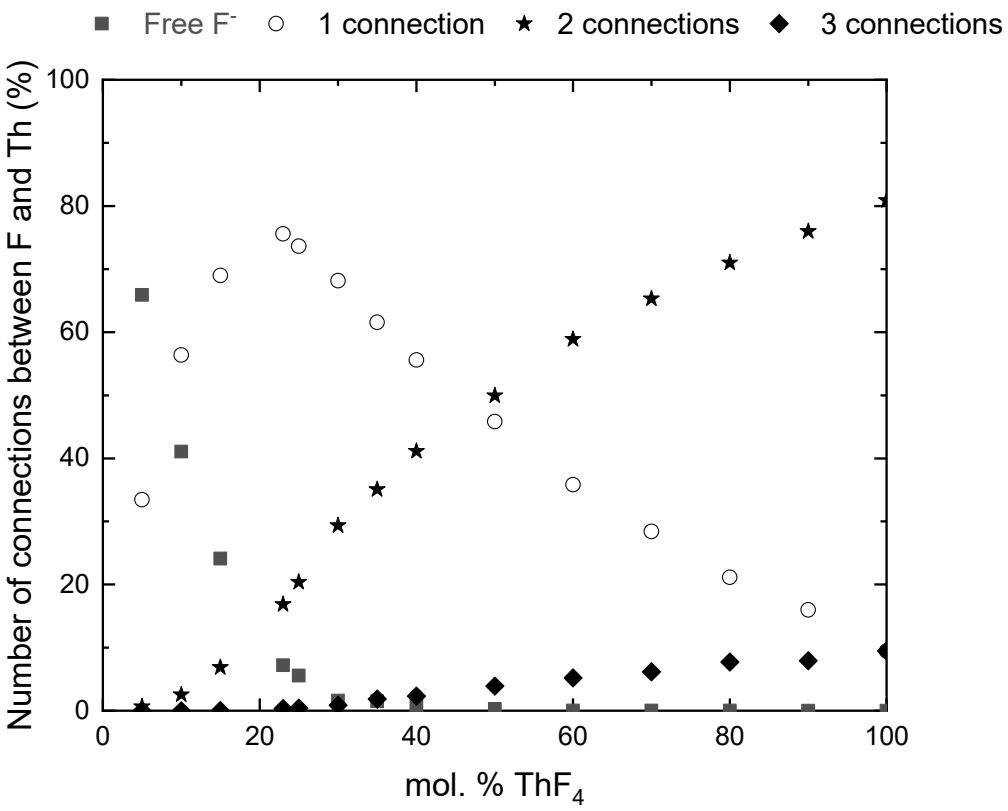
Free F⁻
1 connection
2 connections
3 connections
Number of connections between F and Th (%)
mol. % ThF4
0
20
40
60
80
100

Figure 7

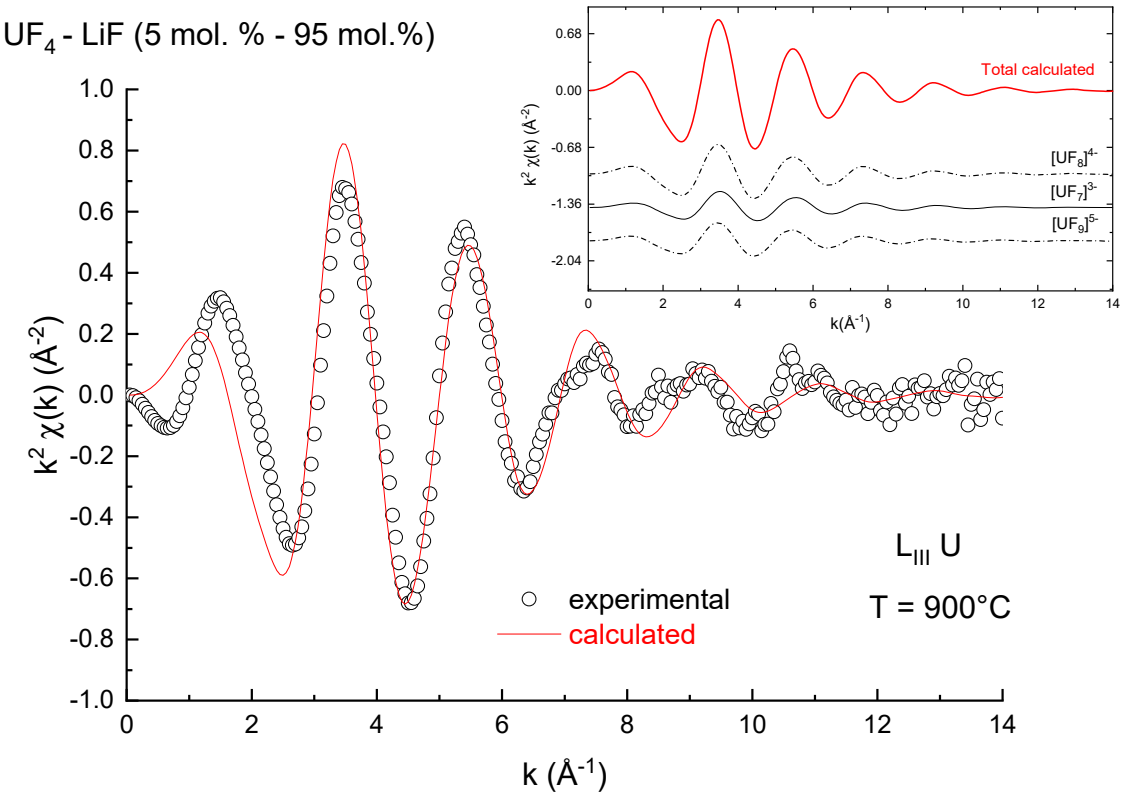

Figure 8

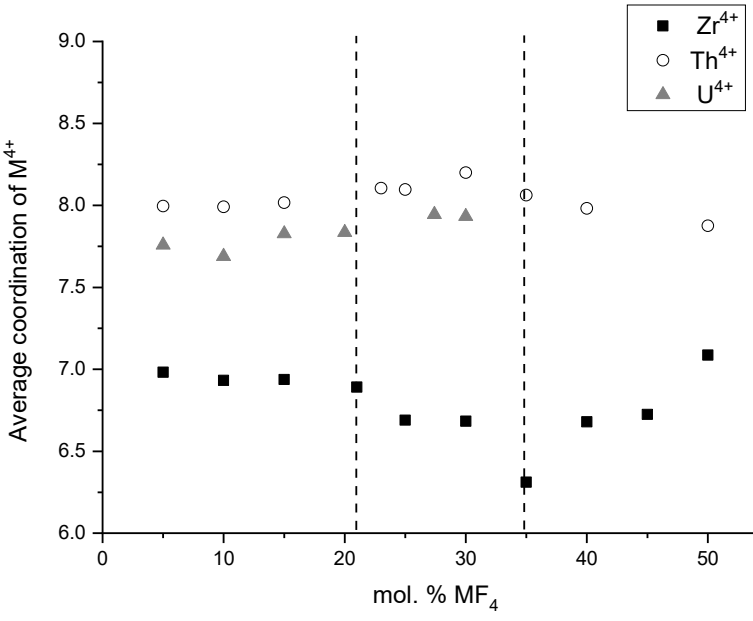

Figure 9

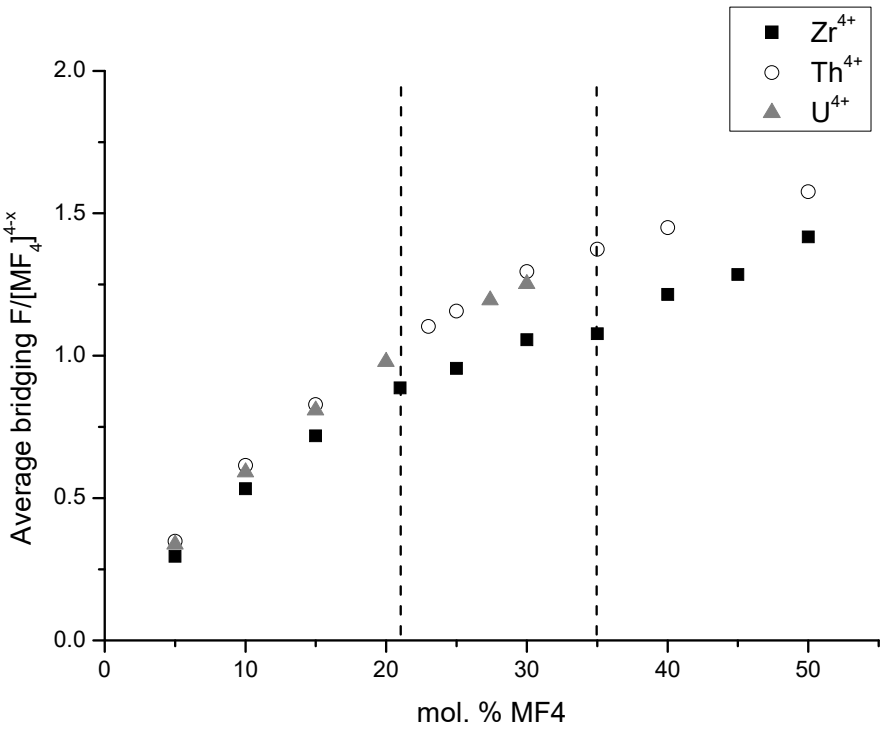
Zr4+
Th4+
U4+
Average bridging F/[MF4]4-x
mol. % MF4
0.0
0.5
1.0
1.5
2.0
0
10
20
30
40
50

Figure 10

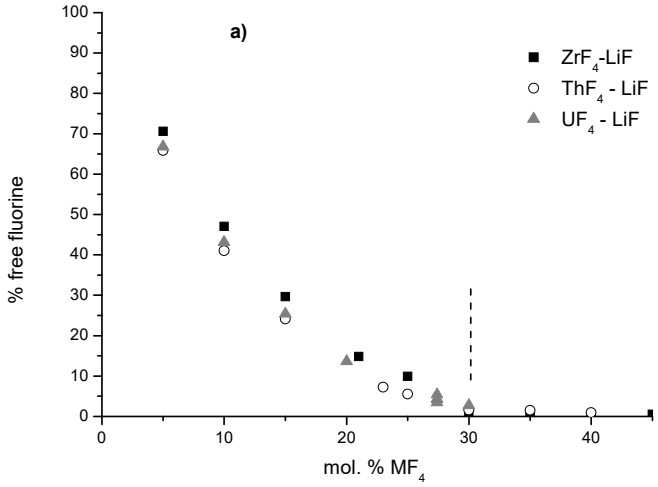
a)
% free fluorine
mol. % MF4
ZrF4-LiF
ThF4 - LiF
UF4 - LiF

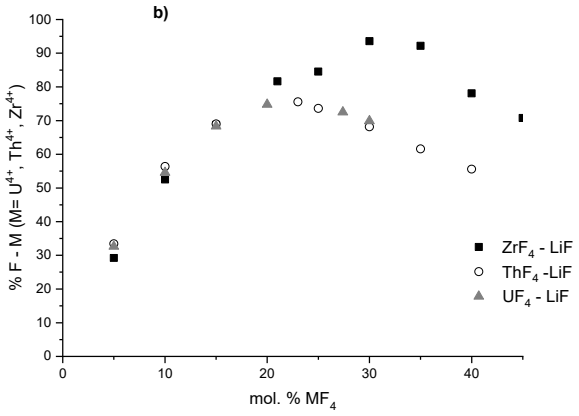
b)
% F - M (M= U4+, Th4+, Zr4+)
mol. % MF4
ZrF4 - LiF
ThF4 -LiF
UF4 - LiF

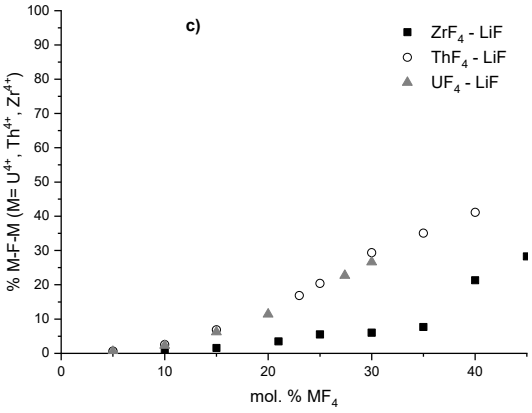
c)
% M-F-M (M= U4+, Th4+, Zr4+)
mol. % MF4
ZrF4 - LiF
ThF4 - LiF
UF4 - LiF

Figure 11

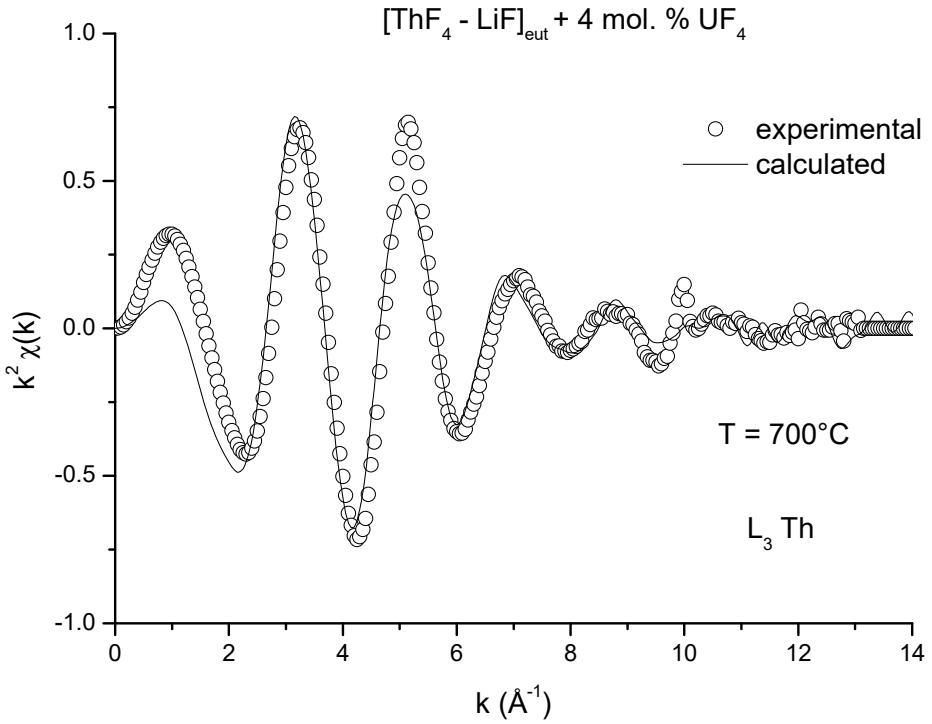

Figure 12

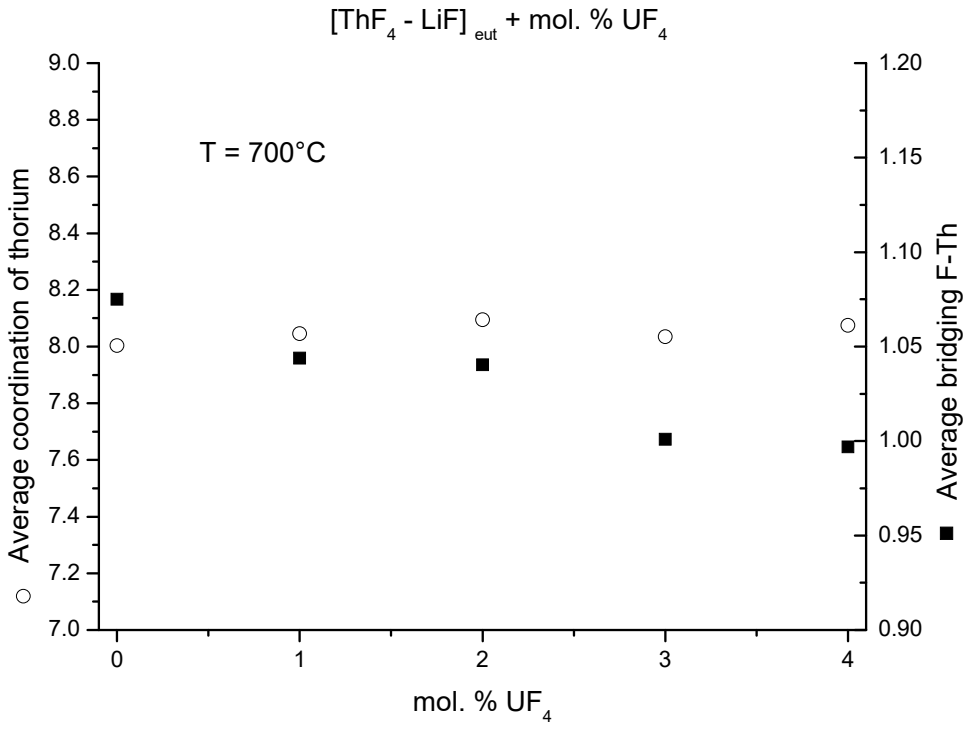

Figure 13

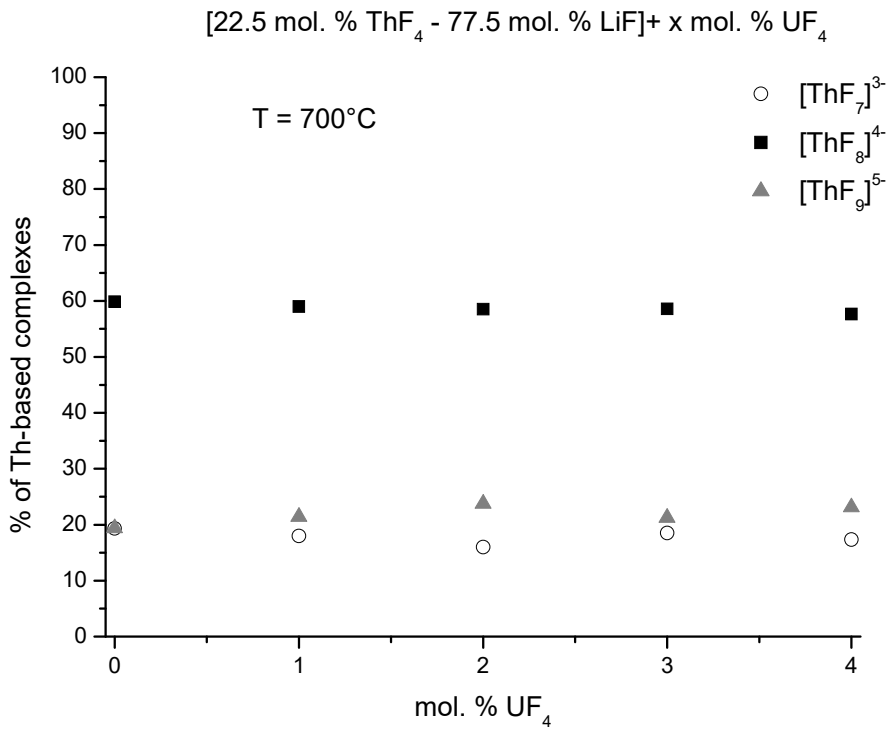

Figure 14

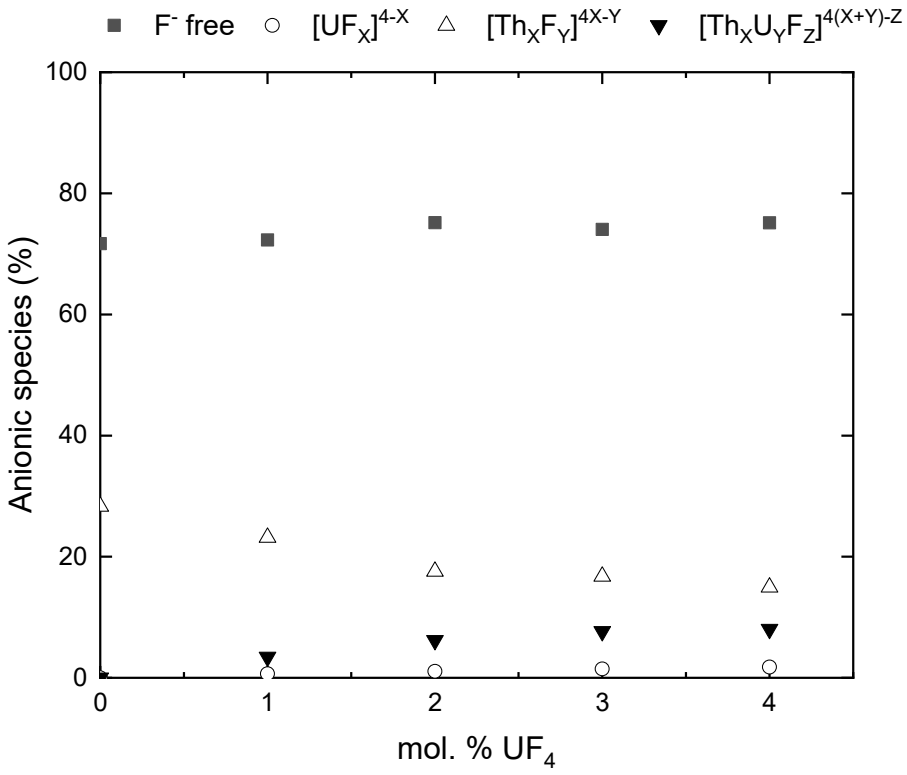

Figure 15

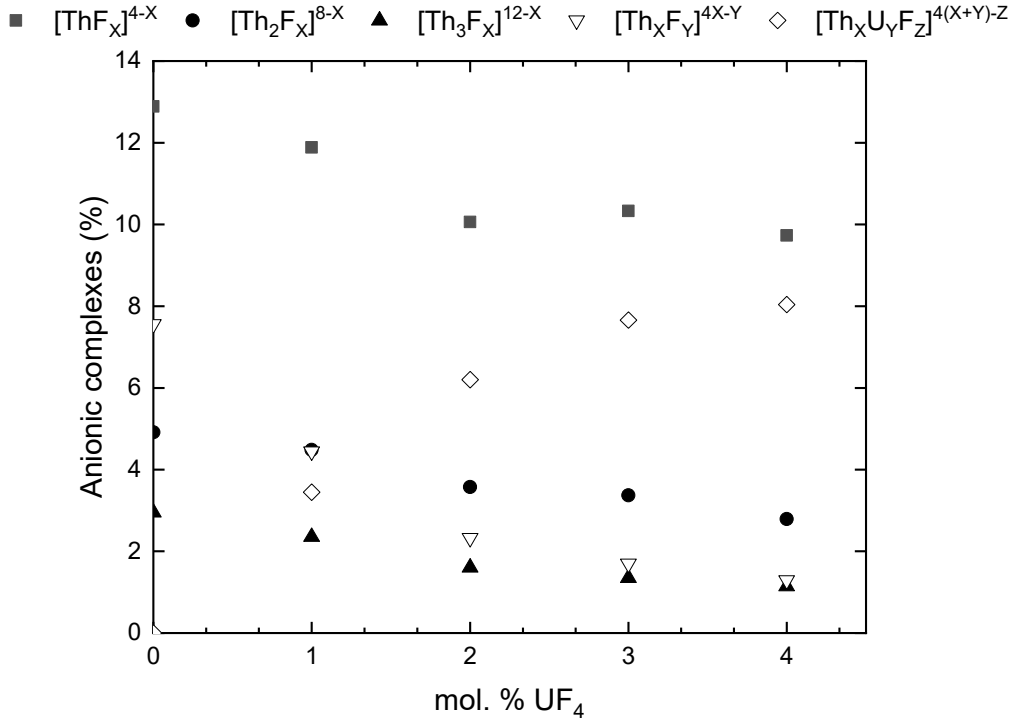
[ThF_X]^4-X
[Th_2F_X]^8-X
[Th_3F_X]^12-X
[Th_XF_Y]^4X-Y
[Th_XU_YF_Z]^4(X+Y)-Z
Anionic complexes (%)
mol. % UF4

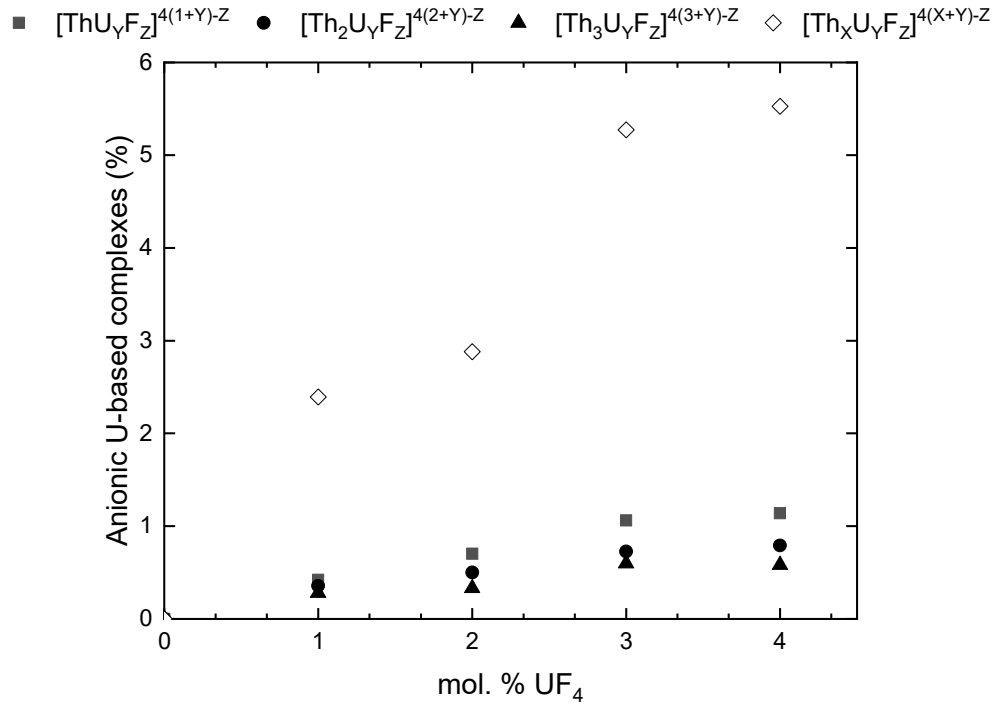
[ThU_YF_Z]^4(1+Y)-Z
[Th_2U_YF_Z]^4(2+Y)-Z
[Th_3U_YF_Z]^4(3+Y)-Z
[Th_XU_YF_Z]^4(X+Y)-Z
Anionic U-based complexes (%)
mol. % UF4

Figure 16

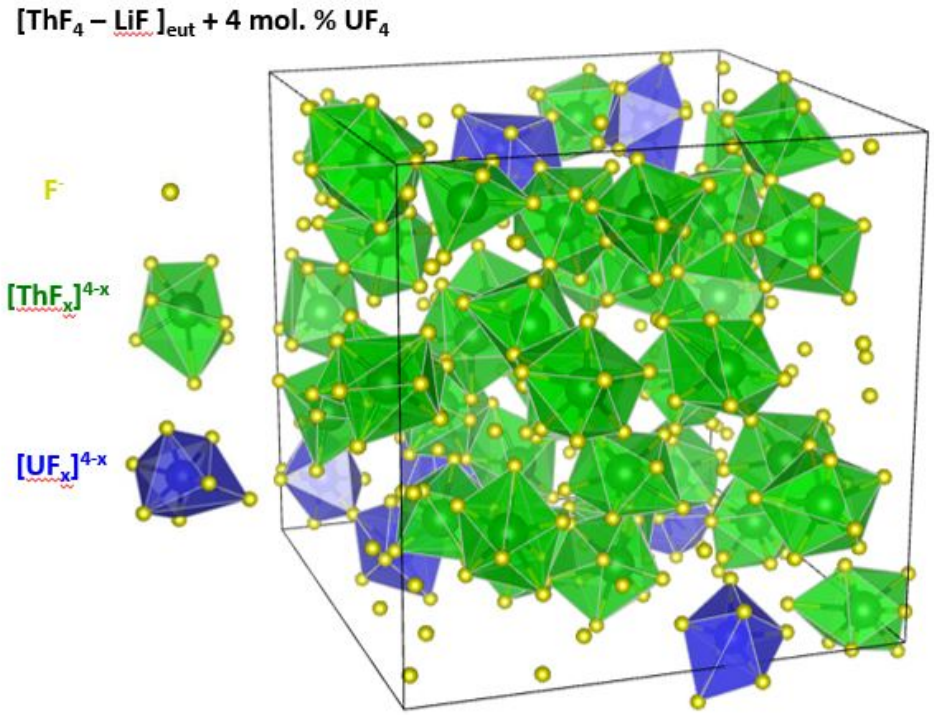

Figure 17

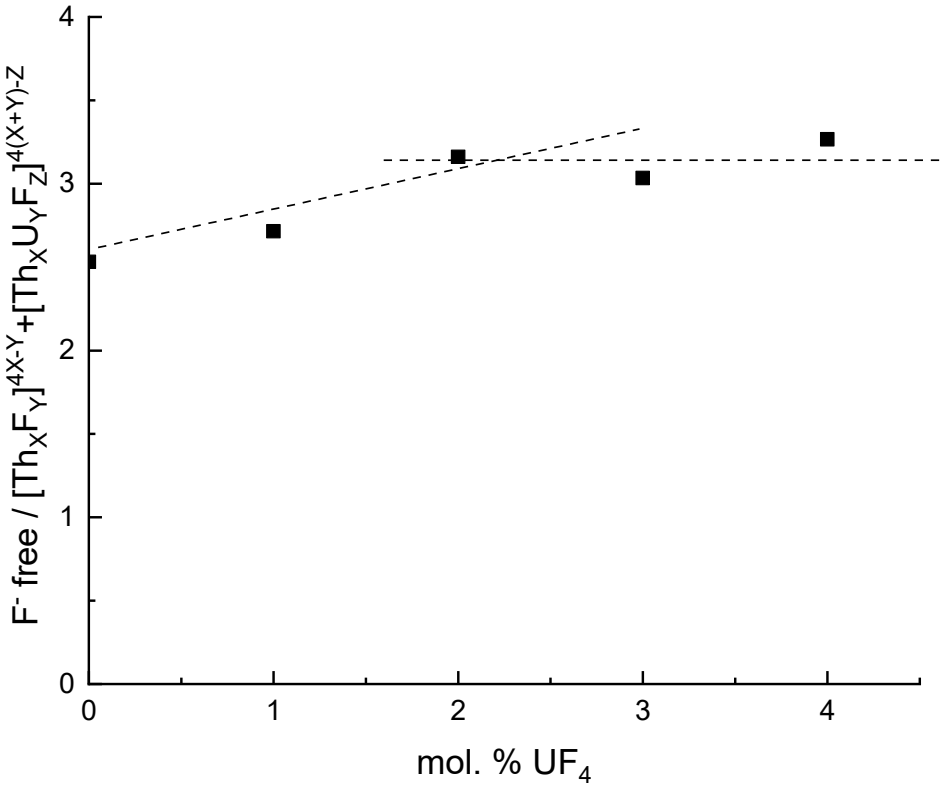

Figure 18

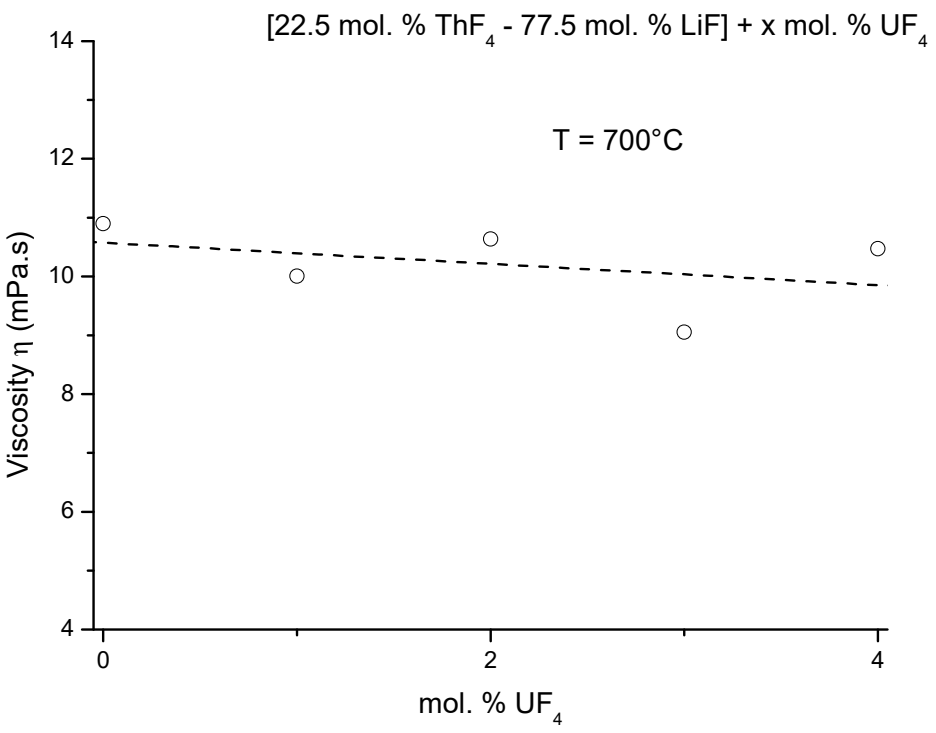
[22.5 mol. % ThF4 - 77.5 mol. % LiF] + x mol. % UF4
T = 700°C
Viscosity η (mPa.s)
14
12
10
8
6
4
0
2
4
mol. % UF4

Figure 19